JACS
JOURNAL OF THE AMERICAN CHEMICAL SOCIETY
Communication
pubs.acs.org/JACS

Universal Sulfide-Assisted Synthesis of M–Ag Heterodimers (M = Pd, Au, Pt) as Efficient Platforms for Fabricating Metal–Semiconductor Heteronanostructures

Su-Un Lee, Jong Wook Hong, Sang-Il Choi, and Sang Woo Han*

Department of Chemistry and KI for the NanoCentury, KAIST, Daejeon 305-701, Korea
Center for Nanomaterials and Chemical Reactions, Institute for Basic Science (IBS), Daejeon 305-701, Korea

Supporting Information

ABSTRACT: We report a universal sulfide-assisted synthesis strategy to prepare dumbbell-like M–Ag heterodimers (M = Pd, Au, Pt). Sulfide ions can give fine control over the reaction kinetics of Ag precursors, resulting in the anisotropic overgrowth of Ag to realize the dumbbell-like heterodimers irrespective of the surface facets or components of the M domain. The M–Ag heterodimers were facilely transformed to M–Ag_2S heterodimers via a simple sulfidation reaction. This study provides a versatile approach to realizing not only metal–metal heterodimers but also semiconductor–metal heterodimers and will pave the way for designing heteronanostructures with unprecedented morphologies and functions.

The modification of nanostructured semiconductor materials by controlling their shape,[1] doping ions,[2] and facets,[3] as well as by hybridizing them with metal nanostructures,[4] has been extensively investigated to develop desirable materials for practical photovoltaic and photocatalytic applications. In particular, semiconductors coupled with various metal materials have demonstrated enhanced photocatalytic activities due to the effective suppression of the charge recombination of the semiconductors by metal domains through accepting photogenerated electrons.[4] To fully exploit the advantages of conjugated metal domains, controlling the facets[5] and components[6] of the metal domains is critical. The surface facets of metal domains associated with their shapes indeed influence the overall catalytic performance of semiconductor–metal hybrid nanostructures because transferred electrons to metal domains participate in catalytic processes.[4a,7] In addition, certain metal components not only trap photogenerated electrons but also strongly affect the catalytic reaction pathway.[8] However, since different metal components have different inherent nucleation and growth habits toward semiconductors, the synthesis of hybrid nanostructures with a well-defined structure has been limited to one or two kinds of metal element for a specific semiconductor system.[6a,9] As such, the development of a universal method for the controlled synthesis of semiconductor–metal hybrid nanostructures irrespective of the facets and components of the metal domains remains a great challenge, and its success can offer a wide selection of hybrid structures for optimizing photocatalytic performance for specifically intended reactions.

Semiconducting Ag_2S nanostructures with a narrow band gap in the range of 1.4–2.3 eV[10] have recently been used in fabricating electronic and optical devices due to their unique properties, such as enhanced optical nonlinearity and near-infrared photoluminescence.[11] However, the synthesis of Ag_2S–metal hybrid nanostructures with tailored morphologies has met with limited success because a lattice strain can be created between the monoclinic crystal structure of Ag_2S and the face-centered cubic (*fcc*) structure of common metal materials, and Ag_2S has a strong tendency to aggregate to yield bulk precipitates.[11a] As an alternative approach, converting Ag in preformed metal–Ag heterodimers to Ag_2S *via* a sulfidation reaction is very promising for generating hybrid nanostructures of Ag_2S.[12] In this regard, several seed-mediated growth methods reported in the literature can be considered as a synthetic protocol to prepare metal–Ag heterodimers.[13−16] However, to our knowledge, there is no general synthetic strategy that can be used in fabricating metal–Ag heterodimers regardless of the metal components. Here, we report a novel seed-mediated synthesis of dumbbell-like metal (M, M = Pd, Au, Pt) nanocube–Ag heterodimers with the assistance of sulfide ions (S^{2-}). S^{2-} ions give fine control over the reaction kinetics of Ag precursors and thereby induce the selective deposition of Ag onto one of the crystal planes of preformed M nanocubes irrespective of the metal components, thus realizing selective shape anisotropy in the form of M nanocube–Ag heterodimers (Scheme 1). Moreover, we also prepared octahedral nanocrystal–Ag

Scheme 1. Schematic Illustration of the Sulfide-Assisted Synthesis of Dumbbell-like M–Ag Heterodimers

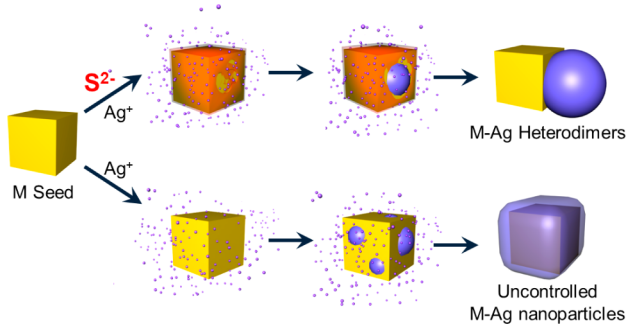

Received: January 18, 2014
Published: March 26, 2014

   dx.doi.org/10.1021/ja500552p | *J. Am. Chem. Soc.* 2014, 136, 5221−5224

heterodimers using the same protocol, thus verifying that the proposed sulfide-assisted synthetic strategy can be a universal method for the controlled synthesis of metal–Ag hybrid nanostructures regardless of the facets or components of the metal domain. Most interestingly, dumbbell-like M nanocrystal–Ag_2S heterodimers could readily be prepared from the M nanocrystal–Ag heterodimers through a facile sulfidation reaction without the aggregation of Ag_2S domains.

In a typical synthesis of M nanocube–Ag heterodimers, Ag precursors ($AgNO_3$) were reduced by ascorbic acid (AA) on presynthesized M nanocubes (Figure S1 in the Supporting Information (SI), where the average edge lengths of Pd, Au, and Pt nanocubes were 30, 58, and 33 nm, respectively) in an aqueous solution of cetyltrimethylammonium chloride (CTAC) in the presence of Na_2S (see experimental details in the SI). Representative transmission electron microscopy (TEM) images of the products are shown in Figure 1a–c, demonstrating the

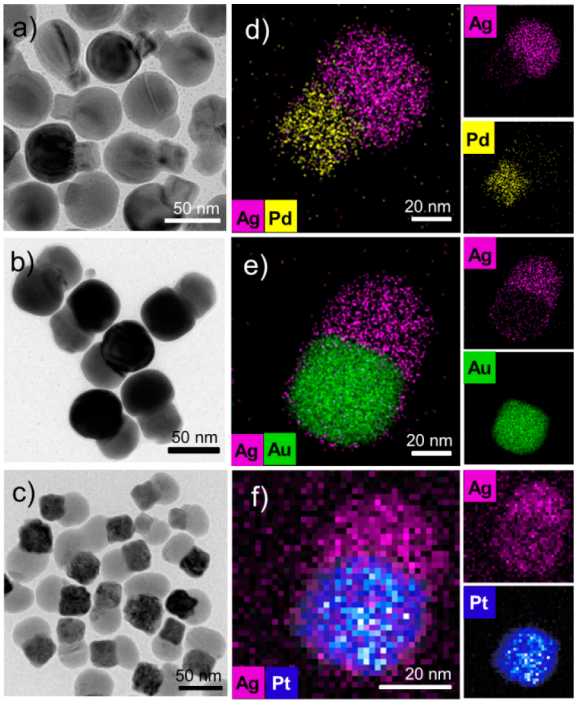

Figure 1. (a–c) TEM and (d–f) HAADF-STEM-EDS elemental mapping images of (a,d) Pd nanocube–Ag heterodimers, (b,e) Au nanocube–Ag heterodimers, and (c,f) Pt nanocube–Ag heterodimers.

successful formation of monodisperse M nanocube–Ag heterodimers through the asymmetric growth of Ag on M nanocubes (see also the scanning electron microscopy (SEM) images of the products shown in Figure S2 in the SI). No homogeneous nucleation of Ag to form Ag nanoparticles was observed in any of the samples. The average sizes of the M nanocube–Ag heterodimers estimated from their long axis lengths were 70, 87, and 66 nm for Pd, Au, and Pt nanocube–Ag heterodimers, respectively. The high-angle annular dark-field scanning TEM-energy-dispersive X-ray spectroscopy (HAADF-STEM-EDS) elemental mapping images of each M nanocube–Ag heterodimer show the distinct compositional distribution of each constituent metal element (Figure 1d–f), unambiguously revealing the heterodimer structure of the products. The X-ray diffraction (XRD) patterns of M nanocube–Ag heterodimers showed characteristic diffraction peaks of individual metal components that can be assigned to the reflections from the *fcc* structure of M and Ag (Figure S3 in the SI).

The presence of the appropriate amount of S^{2-} ions in the reaction medium is the key synthetic lever for the formation of M nanocube–Ag heterodimers. In fact, when the Ag precursors were reduced on as-prepared M nanocubes without S^{2-} ions under otherwise identical synthesis conditions, irregular deposition of Ag on M nanocubes was observed (Figure S4 in the SI), which may be due to the random heterogeneous nucleation of Ag. On the other hand, an excess amount of S^{2-} ions impeded the reduction of Ag precursors (Figure S5 in the SI). On the basis of these findings, it can be assumed that S^{2-} ions control the heterogeneous nucleation of Ag by manipulating the reduction kinetics of Ag^+ ions, which results in the growth of Ag predominantly on one side of the preformed M nanocubes. To verify the effect of S^{2-} ions on the reduction kinetics of Ag^+ ions, the nucleation of Ag on Pd nanocubes was monitored by measuring the UV–vis extinction spectra of reaction solutions with different amounts of S^{2-} ions over the course of the reaction. The intensity of a typical absorption peak of a Ag nanostructure at 420 nm was chosen as an index for the degree of Ag nucleation on M nanocubes. When Ag^+ ions were irregularly reduced on Pd nanocubes in the absence of S^{2-} ions, the nucleation of Ag initiated in 15 min (Figure S6a in the SI). On the hand, the nucleation of Ag was delayed by about 5 min when Pd nanocube–Ag heterodimers were obtained (Figure S6b in the SI). When the amount of S^{2-} ions was increased by 20-fold compared to that used in the standard synthesis, the absorption peak at 420 nm did not appear even after 3 h (Figure S6c in the SI), which reflected the prohibited nucleation of Ag. These results indicate that the reduction kinetics of Ag^+ ions slows as the amount of S^{2-} ions increases, and the control over the reduction/nucleation kinetics of Ag^+ ions is crucial for the formation of M nanocube–Ag heterodimers. This was further confirmed by a control experiment. Namely, when the reduction kinetics of Ag^+ ions was intentionally accelerated by increasing the amount of reductant (AA) by 2-fold, with other conditions kept the same as in the preparation of the Pd nanocube–Ag heterodimers, inhomogeneous nanostructures instead of dumbbell-like heterodimers were generated from the irregular deposition of Ag on Pd nanocubes (Figure S7 in the SI), as observed in the synthesis without S^{2-} ions. It is notable that control over the reduction kinetics of Ag^+ ions solely by changing the amount of AA in the absence of S^{2-} ions did not result in the formation of dumbbell-like M nanocube–Ag heterodimers (Figure S8 in the SI). On the other hand, control over other experimental variables that can modify the nucleation/growth kinetics of Ag, such as the amount of M nanocube precursors, type of surfactant, and reaction temperature, did not alter the growth manner of Ag on the M nanocubes (Figure S9 in the SI).

On the basis of these results and findings, we infer that the random heterogeneous nucleation of Ag can be suppressed in a sulfide-assisted environment because the Ag precursor is prevented from freely approaching the M nanocube surfaces on account of the S^{2-} ions passivating the surface of the nanocubes. It is well-known that sulfide species can passivate Pd, Au, and Pt surfaces due to its binding affinity to metal.[17] The role of sulfide in the formation of M nanocube–Ag heterodimers was further verified by our observation that similar heterodimer structures were generated when other sulfide species, such as NaHS, was used in the synthesis instead of Na_2S (Figure S10 in the SI). Once the nucleation of Ag occurs on a relatively exposed surface of nanocubes, Ag overgrows selectively on one side of the

dx.doi.org/10.1021/ja500552p | *J. Am. Chem. Soc.* 2014, 136, 5221–5224

nanocubes, which leads to the generation of dumbbell-like structures. In fact, TEM measurements on samples taken from early in the reaction confirmed the nucleation of Ag primarily on one side of the nanocubes (Figure S11 in the SI). This proposed formation mechanism is schematically illustrated in Scheme 1.

The proposed sulfide-assisted synthetic strategy is not limited to metal nanostructures with specific facets, though halide ions or surface-stabilizing agents, such as iodide,[18] bromide,[19] citrate,[20] and poly(vinyl pyrrolidone) (PVP),[20] adsorb preferentially on specific surface facets of nanostructures. For instance, when Pd nanooctahedra enclosed by {111} facets (Figure S12 in the SI) were used as seeds instead of Pd nanocubes with {100} facets, Pd nanooctahedron−Ag heterodimers were readily prepared in the same way (Figure S13 in the SI). This demonstrates that the proposed method can be employed generally to generate shape-controlled metal nanostructure−Ag heterodimers irrespective of the kind of component or shape of the metal nanostructures, while previous strategies have not succeeded in fabricating heterodimers with a variety of metal combinations and morphologies.

After the formation of M−Ag heterodimers, passivating S^{2-} ions on the metal domains were effectively removed through repeated washing by centrifugation with deionized water. In fact, sulfur was not detected in the elemental analyses for the purified M−Ag heterodimers using an inductively coupled plasma-atomic emission spectrometer (ICP-AES) (Table S1 in the SI), which indicates that the amount of S atoms adsorbed on the heterodimers was less than the detection limit, if any. Furthermore, X-ray photoelectron spectroscopy (XPS) measurements on the synthesized M−Ag heterodimers revealed that Pd, Au, and Pt exist in single metallic states (Figure S14 in the SI). These results indicate that the inherent surface properties of the metal domains were not modified after the formation of heterodimers.

By using the synthesized M−Ag heterodimers as starting materials, M−Ag_2S heterodimers could readily be prepared through a sulfidation reaction, where Ag was transformed to Ag_2S by reacting the M−Ag heterodimers with an aqueous solution of Na_2S at room temperature (see experimental details in the SI).[12] During the sulfidation reaction, PVP was used as a stabilizer to protect the surface of the Ag_2S domains from aggregation; otherwise, severe agglomeration between heterodimers was observed (Figure S15 in the SI). As shown in Figure 2, M nanocube−Ag_2S heterodimers preserved the original shape of M nanocube−Ag heterodimers overall. The EDS elemental mapping images of each M nanocube−Ag_2S heterodimer further showed that individual components were confined in the form of dumbbell-like heterodimers. In the elemental mapping images of Au− and Pt−Ag_2S heterodimers, the S component seems to be distributed among all the domains. However, this is due to the similar EDS peak position of S (Kα at 2.307 keV) with those of Au (Mα at 2.120 keV) and Pt (Lα at 2.048 keV). The XRD patterns of M nanocube−Ag_2S heterodimers showed characteristic diffraction peaks associated with the monoclinic structure of Ag_2S together with those from the *fcc* structure of Pd, Au, and Pt, while no peak from the Ag was observed (Figure 3), which unambiguously reveals the successful formation of M nanocube−Ag_2S heterodimers without the transformation of M components into corresponding metal sulfides. On the other hand, Pd nanooctahedron−Ag heterodimers could also be converted successfully into Pd nanooctahedron−Ag_2S heterodimers *via* the sulfidation reaction (Figure S16 in the SI).

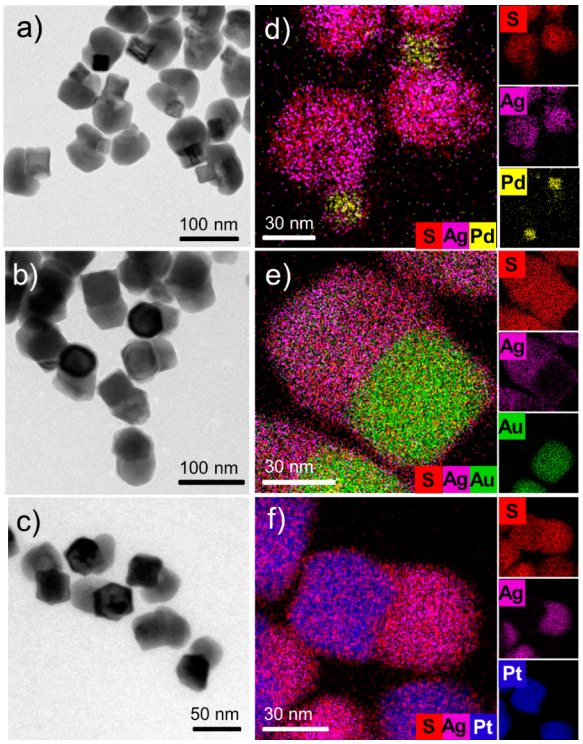

Figure 2. (a−c) TEM and (d−f) HAADF-STEM-EDS elemental mapping images of (a,d) Pd nanocube−Ag_2S heterodimers, (b,e) Au nanocube−Ag_2S heterodimers, and (c,f) Pt nanocube−Ag_2S heterodimers.

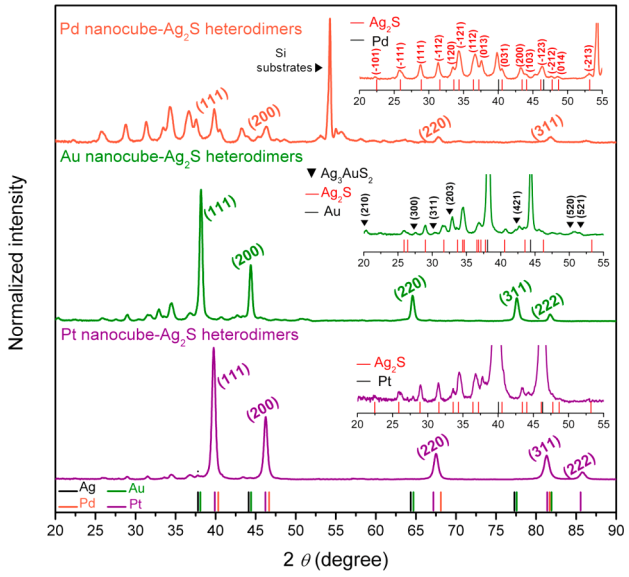

Figure 3. XRD patterns of M nanocube−Ag_2S heterodimers. The magnified XRD patterns in the range 20°−55° in insets show the characteristic diffraction peaks associated with the monoclinic structure of Ag_2S. The positions of Pd, Au, Pt, Ag, Ag_2S, and Ag_3AuS_2 references were taken from the JCPDS database (Pd: 65-6174, Au: 65-2870, Pt: 04-0802, Ag: 04-0783, Ag_2S: 14-0072, Ag_3AuS_2: 33-0587).

In summary, we developed a universal sulfide-assisted method to synthesize dumbbell-like M−Ag heterodimers. In this method, sulfide ions play a pivotal role in tailoring the nucleation kinetics of Ag onto preformed metal nanocrystals, resulting in the anisotropic overgrowth of heteronanostructures to realize the dumbbell-like heterodimers. Despite the different growth

dx.doi.org/10.1021/ja500552p | J. Am. Chem. Soc. 2014, 136, 5221−5224

behaviors of Ag toward various metal components and surface facets, the proposed method produces the heterodimer type of nanomaterials for different metal nanostructures in the identical synthesis route. The prepared dumbbell-like M−Ag heterodimers were easily converted to M−Ag_2S heterodimers through the sulfidation reaction. This work provides a versatile approach to generating not only metal−metal heterodimers but also semiconductor−metal heterodimers and can be extended to designing anisotropic nanomaterials with unprecedented morphologies and functions. Remarkably and as an example, M−Ag_2S heterodimers can be used as an efficient platform to generate M−CdS heterodimers via a cationic exchange reaction within their Ag_2S domains (Figure 4).[21]

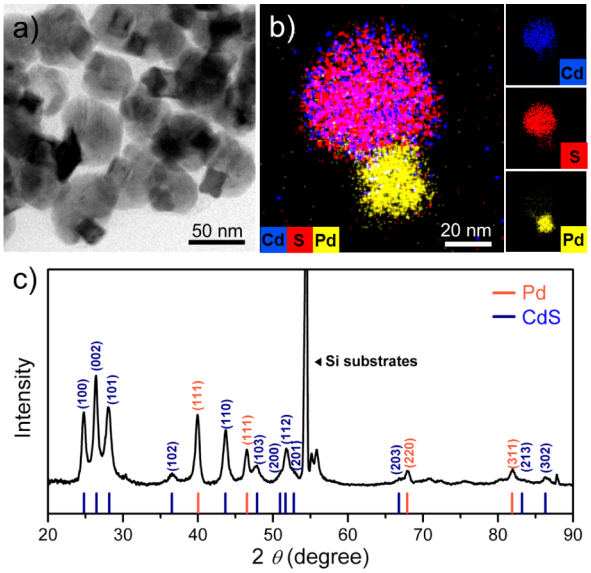

Figure 4. (a) TEM and (b) HAADF-STEM-EDS elemental mapping images of Pd nanocube−CdS heterodimers. (c) XRD pattern of Pd nanocube−CdS heterodimers. The positions of Pd and CdS references were taken from the JCPDS database (Pd: 65-6174, CdS: 41-1049).

■ ASSOCIATED CONTENT

Ⓢ Supporting Information

Experimental details and additional data. This material is available free of charge via the Internet at http://pubs.acs.org.

■ AUTHOR INFORMATION

Corresponding Author

sangwoohan@kaist.ac.kr

Notes

The authors declare no competing financial interest.

■ ACKNOWLEDGMENTS

This work was supported by Basic Science Research Programs (2010-0029149) and the EPB Center (2008-0061892) through the NRF funded by the Korea government (MSIP) and was also supported by Institute for Basic Science (IBS) [CA1301].

■ REFERENCES

(1) (a) Huang, W.-C.; Lyu, L.-M.; Yang, Y.-C.; Huang, M. H. *J. Am. Chem. Soc.* **2012**, *134*, 1261. (b) Cho, I. S.; Chen, Z.; Forman, A. J.; Kim, D. R.; Rao, P. M.; Jaramillo, T. F.; Zheng, X. *Nano Lett.* **2011**, *11*, 4978.

(2) (a) Chen, X.; Liu, L.; Yu, P. Y.; Mao, S. S. *Science* **2011**, *331*, 746. (b) Asahi, R.; Morikawa, T.; Ohwaki, T.; Aoki, K.; Taga, Y. *Science* **2001**, *293*, 269. (c) Liu, M.; Qiu, X.; Miyauchi, M.; Hashimoto, K. *J. Am. Chem. Soc.* **2013**, *135*, 10064.

(3) (a) Jiang, J.; Zhao, K.; Xiao, X.; Zhang, L. *J. Am. Chem. Soc.* **2012**, *134*, 4473. (b) Pan, J.; Liu, G.; Lu, G. Q.; Cheng, H.-M. *Agnew. Chem., Int. Ed.* **2011**, *50*, 2133. (c) Xinag, Q.; Yu, J.; Jaroniec, M. *Chem. Commun.* **2011**, *47*, 4532.

(4) (a) Kim, S. M.; Lee, S. J.; Kim, S. H.; Kwon, S.; Y, K. J.; Song, H.; Somorijai, G. A.; Park, J. Y. *Nano Lett.* **2013**, *13*, 1352. (b) Chen, X.; Shen, S.; Guo, L.; Mao, S. S. *Chem. Rev.* **2010**, *110*, 6503.

(5) (a) Cui, E.; Lu, G. *J. Phys. Chem. C* **2013**, *117*, 26415. (b) Shiraishi, Y.; Fujiwara, K.; Sugano, Y.; Ichikawa, S.; Hirai, T. *ACS Catal.* **2013**, *3*, 312.

(6) (a) Yang, J.; Yinag, J. Y. *Angew. Chem., Int. Ed.* **2011**, *50*, 4367. (b) Wu, M.-C.; Hiltunen, J.; Sápi, A.; Avila, A.; Larsson, W.; Liao, H.-C.; Huuhtanen, M.; Tóth, G.; Shchukarev, A.; Laufer, N.; Kukovecz, Á.; Kónya, Z.; Mikkola, J.-P.; Keiski, R.; Su, W.-F.; Chen, Y.-F.; Jantunen, H.; Ajayan, P. M.; Vajtai, R.; Kordás, K. *ACS Nano* **2011**, *5*, 5025. (c) Zhang, N.; Liu, S.; Fu, X.; Xu, Y.-J. *J. Phys. Chem. C* **2011**, *115*, 9136. (d) Ohyama, J.; Yamamoto, A.; Teramura, K.; Shishido, T.; Tanaka, T. *ACS Catal.* **2011**, *1*, 187.

(7) Mahmoud, M. A.; Qian, W.; El-sayed, M. A. *Nano Lett.* **2011**, *11*, 3285.

(8) (a) Tanaka, A.; Hashimoto, K.; Kominami, H. *J. Am. Chem. Soc.* **2014**, *136*, 586. (b) Wang, Y.-G.; Yoon, Y.; Glezakou, V.-A.; Li, J.; Rousseau, R. *J. Am. Chem. Soc.* **2013**, *135*, 10673. (c) Su, R.; Tiruvalam, R.; He, Q.; Dimitratos, N.; Kesavan, L.; Hammond, C.; Lopez-Sanchez, J. A.; Bechstein, R.; Kiely, C. J.; Hutchings, G. J; Besenbacher, F. *ACS Nano* **2012**, *6*, 6284.

(9) (a) Pang, M.; Hu, J.; Zeng, H. C. *J. Am. Chem. Soc.* **2012**, *132*, 10771. (b) Pradhan, S.; Ghosh, D.; Chen, S. *ACS Appl. Mater. Inter.* **2009**, *1*, 2060. (c) Kuo, C.-H.; Hua, T.-E.; Huang, M. H. *J. Am. Chem. Soc.* **2009**, *131*, 17871.

(10) Hong, X.; Yin, Z.; Fan, Z.; Tay, Y.-Y.; Chen, J.; Du, Y.; Xue, C.; Chen, H.; Zhang, H. *Small* **2014**, *10*, 479.

(11) (a) Kim, Y.-Y.; Walsh, D. *Nanoscale* **2010**, *2*, 240. (b) Jiang, P.; Tian, Z.-Q.; Zhu, C.-N; Zhang, Z.-L.; Pang, D.-W. *Chem. Mater.* **2012**, *24*, 3.

(12) (a) Zeng, J.; Tao, J.; Su, D.; Zhu, Y.; Qin, D.; Xia, Y. *Nano Lett.* **2011**, *11*, 3010. (b) Seo, D.; You, C. I.; Jung, J.; Song, H. *J. Am. Chem. Soc.* **2008**, *130*, 2940.

(13) (a) Zeng, J.; Zhu, C.; Tao, J.; Jin, M.; Zhang, H.; Li, Z.-Y.; Zhu, Y.; Xia, Y. *Angew. Chem., Int. Ed.* **2012**, *51*, 2354. (b) Zhu, C.; Zeng, J.; Tao, J.; Johnson, M. C.; Schmidt-Krey, I.; Blubaugh, L.; Zhu, Y.; Gu, Z.; Xia, Y. *J. Am. Chem. Soc.* **2012**, *134*, 15822.

(14) Xing, S.; Feng, Y.; Feng, Y.; Tay, Y. Y.; Chen, T.; Xu, J.; Pan, M.; He, J.; Hng, H. H.; Yan, Q.; Chen, H. *J. Am. Chem. Soc.* **2010**, *132*, 9537.

(15) Feng, Y.; He, J.; Wang, H.; Tay, Y. Y.; Sun, H.; Zhu, L.; Chen, H. *J. Am. Chem. Soc.* **2012**, *134*, 2004.

(16) Lee, J.-H.; Kim, G.-H.; Nam, J.-M. *J. Am. Chem. Soc.* **2012**, *134*, 5456.

(17) (a) Koczkur, K.-M.; Hamed, E. M.; Houmam, A. *Langmuir* **2011**, *27*, 12270. (b) Baldyga, L. M.; Blavo, S. O.; Kuo, C.-H.; Tsung, C.-K.; Kuhn, J. N. *ACS Catal.* **2012**, *2*, 2626. (c) Liu, Y.; Sun, C.; Bolin, T.; Wu, T.; Liu, Y.; Sternberg, M.; Sun, S.; Lin, X.-M. *Nano Lett.* **2013**, *13*, 4893. (d) Tada, H.; Soejima, T.; Ito, S.; Kobayashi, H. *J. Am. Chem. Soc.* **2004**, *126*, 15952.

(18) Ha, T. H.; Koo, H.-J.; Chung, B. H. *J. Phys. Chem. C* **2007**, *111*, 1123.

(19) Peng, H.-C.; Xie, S.; Park, J.; Xia, X.; Xia, Y. *J. Am. Chem. Soc.* **2013**, *135*, 3780.

(20) Zeng, J.; Xia, X.; Rycenga, M.; Henneghan, P.; Li, Q.; Xia, Y. *Angew. Chem., Int. Ed.* **2011**, *50*, 244.

(21) Seo, D.; Park, G.; Song, H. *J. Am. Chem. Soc.* **2012**, *134*, 1221.